



Investigating the performance of reciprocating high-pressure pumps in constant recovery small RO desalination plants

Tamer A. El-Sayed^{a,*}, Amr A. Abdel Fatah^b

^aDepartment of Mechanical Design, Faculty of Engineering, Mataria, Helwan University, Egypt,
email: tamer_alsayed@m-eng.helwan.edu.eg

^bMechanical Department, Faculty of Engineering British University, Egypt, email: amr.abdelkader@bue.edu.eg

Received 25 June 2008; Accepted 30 November 2018

ABSTRACT

Small-scale reverse osmosis plants that can produce less than 50 m³/d are vital for small communities in villages located in remote areas. The design parameters of such plants involve low flow rate and high-pressure feed. For such operating conditions, reciprocating pumps are more favorable than centrifugal pumps because the efficiency of centrifugal pumps in such conditions is reduced extensively. Recently, reciprocating pumps with energy recovery are presented by several pump companies for desalination applications. The concept of energy recovery in these pumps is quite similar to that used in pressure exchangers. In these pumps, the pressurized brine is directed to the back of the pumping pistons which reduces the pumping motor required power. This work presents a numerical simulation and experimental analysis for such pumps. The numerical simulation includes a computational fluid dynamics transient analysis for the used pump. The analysis is presented using both two-dimensional and three-dimensional models. The effects of the operational and design parameters on the performance of the pump and its volumetric efficiency are investigated. The results show that increasing the valve spring stiffness increases the volumetric efficiency. It also shows that increasing the outlet pressure and piston speed reduces the volumetric efficiency. The most striking result to emerge from the data is that reducing the valve spring stiffness below a specific value results in large reduction on the volumetric efficiency. Results of pump's testing at different operating conditions are evaluated. The results of the presented numerical simulation were compared with the experimental results at several operating conditions, and the deviation was less than 10%.

Keywords: Small RO desalination plant; Computational fluid dynamics; Reciprocating pumps; Energy recovery device.

1. Introduction

Reverse osmosis (RO) is one of the most popular processes used for seawater desalination. In the RO process, a semipermeable membrane is used to separate the salts from the water at high-operating pressure depends on the salinity of the feedwater. The growing needs for drinking water for small communities or villages in remote coastal area with access to great amount of seawater motivate the need to small-scale desalination plants that can produce less than 50 m³/d of drinking water [1–3]. These small RO systems

are mostly operated under constant feed pressure. In such case, the recovery ratio varies according to the salinity and temperature of the feed stream. The limited availability of cost-effective energy recovery devices for these small systems causes brine energy to be lost. Consequently, recovery ratios and the associated feed pressures are kept as high as possible to maximize the permeate production. Salt rejection rates of today's RO membranes generally range from 99.4% to 99.8% [4], increasing system recovery ratio reduces the amount of water required to dilute the higher concentration of salts in the brine stream. When the brine solubility limit is

* Corresponding author.

exceeded, salts start to form scale foulants on the surface of the membrane.

In some cases, even a small increase in system recovery can cause the solubility limit of one or more salts to be exceeded and result in higher membrane fouling rates. Membrane scale fouling causes the restriction of water passages and requires increased feed pressure to sustain acceptable permeate production. This results in increasing specific energy consumption (SEC) and reducing system efficiency. Dissolved salts in the brine stream should be diluted by reducing system recovery. Generally, chemical cleaning is used to remove the scale foulants and restore the membrane permeation performance [5,6]. Exceeding salts solubility limits continually due to high recovery ratio requires repeated chemical membrane cleaning thus increasing operation costs of the plant. Additionally, some salt-scale foulants are abrasive and can cause physical damage of membrane surfaces resulting in a reduced operational life. Accordingly, the correlation between soluble salts concentrations as well as the system recovery ratio should be considered for successful and efficient operation of RO plants.

Selecting a small RO plant with constant small recovery ratio can allow for eliminating the possibility of exceeding salts solubility limits.

High-pressure pumps are one of the main components of any desalination plants. It is used to boost the feed pressure to the required permeation pressure. These pumps are either centrifugal or reciprocating pumps [7–9]. The advantage of reciprocating pumps over centrifugal pumps is evident at very low flow rate ranges where the efficiency of centrifugal pumps deteriorates considerably [10,11]. On the other hand, the reciprocating pumps flow is independent of the outlet pressure. The main drawback of the reciprocating pumps is the discharge flow pulsations which arise from the nature of the flow entering and leaving the pump. This can be reduced by using multiple plunger pumps as well as pulsation dampers [12–14]. Because the main focus of this research is small RO plants which involve small flow rate and high outlet pressure. This results in a very small specific speed as shown in Eq. (1). These conditions motivate the use of reciprocating pump in such application.

$$N_s = \frac{n\sqrt{Q_f}}{H^{0.75}} \quad (1)$$

where N_s is pump specific speed, Q_f is the feed flow rate, n is the pump rotating speed, and H is the pump head.

Recently, energy efficient positive displacement reciprocating high-pressure pumps for small RO plants were developed [15–21]. The design of these pumps showed remarkable energy efficiency. In these pumps, the brine stream is returned to flow into the pump head where it acts on the other side of the pump pistons. The resulting back force reduces the loading of the pump motor and improves the SEC considerably. To simplify the design of these high-pressure pumps, the volume of water being pressurized by the piston's upper side and the volume of the returning brine to the piston's underside are constant. This design feature means that the associated RO system is a constant recovery ratio system. The feed pressure to the membranes will vary according to feed

salinity and feed temperature. Selecting a proper recovery ratio will ensure that salts solubility limits are not exceeded, and the possibility of membranes scale fouling is dramatically reduced.

The main objective of this paper is to investigate the different efficiencies encountered with energy efficient reciprocating high-pressure pumps with constant recovery RO plants. The study is based on numerical simulation and experimental treatments. The introduction section discusses the consequences of high recovery ratio on RO membrane fouling and the importance of using reciprocating pumps in small RO plants. Section 2 of this paper presents the main design features of the pump under consideration. Section 3 presents a model for the pump as well as the computational fluid dynamics (CFD) analysis for determining the volumetric efficiency. Section 4 introduces the experimental study of a small constant recovery RO plant at different operating conditions. These results were used to validate the introduced model.

2. Main design features of the pump

In this work, the performance of a small power triplex reciprocating high-pressure pump is investigated in RO desalination. The design of this pump incorporated an integrated energy recovery feature that allows the pressurized brine stream coming from the membranes to apply a back force on the pistons undersides. This back force will reduce the electric consumption of the pump's motor. Fig. 1 presents a schematic description for a single piston of the high-pressure pump, while Table 1 presents the main design specifications of the pump.

The ratio between the volume in the underside cylinder and the volume of cylinder above the piston is designed to suit the plant recovery ratio. In the suction stroke, the check valves of the feed as well as the brine drain allow the unpressurized stream to enter the pump's head and the brine stream to be drained. During the discharge stroke, the check valves of the pressurized feed as well as the pressurized brine are open. The feedwater is subject to the net force applied by the piston resulting from the electric motor and back pressure of the brine stream. Accordingly, the pressure begins to rise until the permeation of the feed stream is forced to start through the membranes.

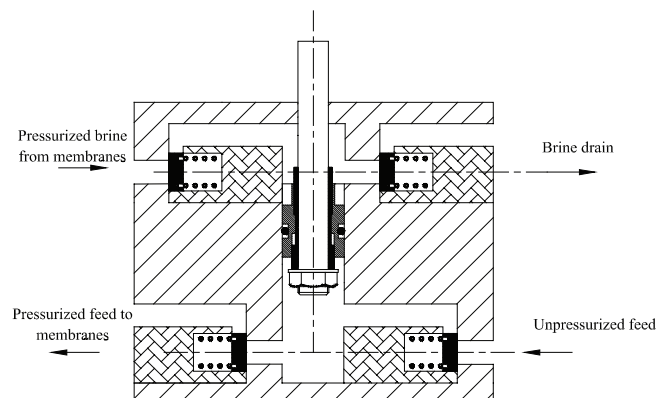


Fig. 1. Schematic description of a single piston/cylinder.

Table 1
Main design specifications of the pump

Parameter	Value
Feed flow rate, m ³ /h	1.25
Piston diameter, mm	25
Piston stroke, mm	16
Maximum discharge head, m	600
Maximum speed, rpm	735
Maximum recovery ratio, %	35
Minimum recovery ratio, %	30
Frame load, bar	70
Limit speed, rpm	1,400
Motor	3 phase
Motor rated power, HP	2
Motor speed (60 HZ), rpm	1,725

3. Modeling the performance of the reciprocating pump

A model that describes the performance of the pump is developed. A balance of power at a specific feed salinity gives that the consumed electrical power should equal the power required to pressurize the feed stream minus the power resulting from the brine energy recovery. Eqs. (2)–(4) introduce the described power balance [11,22,23].

$$P_{\text{net}} = P_p - P_r = I \cdot V \quad (2)$$

$$P_p = \eta_v \cdot Q_f \cdot H_f \cdot g \cdot \rho_f / \eta_p \quad (3)$$

$$P_r = (1-R) \cdot \eta_v \cdot Q_f \cdot H_r \cdot g \cdot \rho_b \cdot \eta_r \quad (4)$$

where P_{net} is the net power; P_p is the pump power, P_r is the energy recovery power, R is the recovery ratio, η_p is the power pump overall efficiency, η_r is the hydraulic efficiency of the energy recovery mechanism, η_v is the pump volumetric efficiency and ρ_f , ρ_b are the feed and brine densities.

The overall efficiency of the pump comprises the efficiency of the electric motor, the efficiency of the power transmission system as well as the mechanical efficiency of the reciprocating pump such that:

$$\eta_p = \eta_m \cdot \eta_t \cdot \eta_h \quad (5)$$

The recovery efficiency is equal to the mechanical efficiency as the motor and the transmission efficiencies are not involved in the recovery cycle.

$$\eta_r = \eta_m \quad (6)$$

The mechanical efficiency of a power reciprocating pump varies as a function of the frame load percentage [16]. The frame load percentage is expressed by the ratio of the applied feed pressure over the pressure rating of the pump. Higher frame load percentage increases the mechanical efficiency as shown in Fig. 2. Reciprocating pumps have mechanical efficiencies up to 87%. The associated losses are due to friction in the stuffing box seals and check valves.

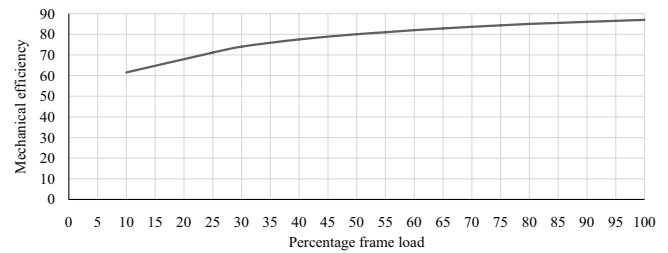


Fig. 2. Mechanical efficiency vs. frame load [13].

3.1. The volumetric efficiency

The volumetric efficiency is the other constituent of a reciprocating pump efficiency. It is one of the crucial elements of the evaluation of the reciprocating pump performance. The volumetric efficiency is defined as the ratio of the actual output flow rate to the theoretical displacement of the pump [23]. Volumetric efficiency is expressed in terms of the working fluid compressibility, feed pressure differential, pump chamber clearance to displacement ratio and check valves slippage loss [11,13] as indicated in Eq. (7).

$$\eta_v = [1 - H_f \cdot v_c \cdot \beta \cdot (C/D)] / (1 - H_f \cdot v_c \cdot \beta) - S \quad (7)$$

where β is the water compressibility, C/D is chamber clearance volume to displacement volume ratio, S is the check valves loss due to water slippage, and v_c is water specific weight.

3.2. CFD analysis

CFD can be used to model the functionality of hydraulic machines. This enables deep understanding of their performance and subsequent improvement of their efficiencies. CFD has proven to be beneficial in the modeling of centrifugal pumps and turbines, compressors, fans, and valves [24–31]. The CFD analysis can be divided to quasi-steady state and transient analysis. The transient analysis is generally more complicated than the quasi-steady state analysis and consumes more computational time. Quasi-steady state analysis is used when the change of the operating conditions is very small such as the centrifugal pump and fans operation [32,33]. Examples of the transient analysis are the centrifugal pump start-up and shut down and the reciprocating pump operation. Modeling the operation of reciprocating pumps dictates a transient CFD analysis. It includes the reciprocating motion of the pump plunger or piston and the opening and closure of the suction and discharge valves [29,30].

Through this work, both two- and three-dimensional transient CFD analyses are conducted. The pump 2D and 3D models are created based on the design specifications of RO plant which are listed in Table 1. The 2D and 3D models are then exported to ANSYS design modeler. The models are then transferred to ANSYS mesh module. Fig. 3(a) shows the two-dimensional model domains, and Fig. 3(b) shows a half section through the three-dimensional fluid domain for the reciprocating pump. Each model is divided into stationary and dynamic domains. The movable domains are the piston and the two valves. The difference between the

two-dimensional model and the three-dimensional analysis is that in the two-dimensional model the investigated section (see Fig. 3(a)) has a uniform depth of 1 m. Therefore, in the two-dimensional analysis all the system inputs and outputs based on the cross section area should be scaled by the ratio of section area based on unit depth to the ratio of the real section area. This includes the valve mass, valve spring stiffness, inlet and outlet flow rates, and the valve forces. Due to the symmetry of the three-dimensional model, only half model is investigated as shown in Fig. 3(b). This reduces the mesh size into half and reduces the computational time as well.

The developed CFD models involve the motion of the pump’s piston as well as the motion of the check valves. The governing equation for the piston motion is given by Eqs. (8) and (9).

$$V_y = a \times \sin\left(\frac{2\pi N}{60} t\right) \tag{8}$$

$$a = \frac{\pi L_s N^2}{60} \tag{9}$$

where N is the motor speed in rpm, L_s = is the stroke length, and t is the time.

Figs. 4 and 5 show the piston velocity in m/s and piston displacement in m through one cycle.

The kinetics of the check valves is governed by the balance of the hydraulic and mechanical forces and is given by Eqs. (10) and (11).

$$F_i = F_i + F_s + F_h + F_g \tag{10}$$

$$F_s = k \times y_v, F_g = m \times g, F_i = m \times a \tag{11}$$

where F_i is the preload force, F_s is the spring force, F_h is the hydraulic forces, F_g is the gravity force, k is the valve spring stiffness, Y_v is the valve displacement, m is the valve mass, a is the valve acceleration, and g is the gravity acceleration.

Eqs. (10) and (11) allow for the evaluation of the valve acceleration a . The velocity of the valve can be calculated from the numerical integration of the acceleration over the time. The valves displacements are constrained between the closed position and the full opening position which is 3 mm for the pump under consideration.

3.3. Solver setup

ANSYS Fluent module is used to solve this problem. The solver type is pressure-based and the analysis type is transient. The turbulence model is k -Omega SST. A list of the settings used in the Fluent module is listed in Table 2. The dynamic mesh analysis in the reciprocating pistons and the valves are controlled through a user-defined functions that comprises the introduced models for the piston and check valves. The code of these functions is written in C++ language and then compiled into fluent to control the mesh dynamics. The number of steps is selected to cover the simulation of one and half period. The first half cycle is ignored in the analysis because it includes a period of instability at the start

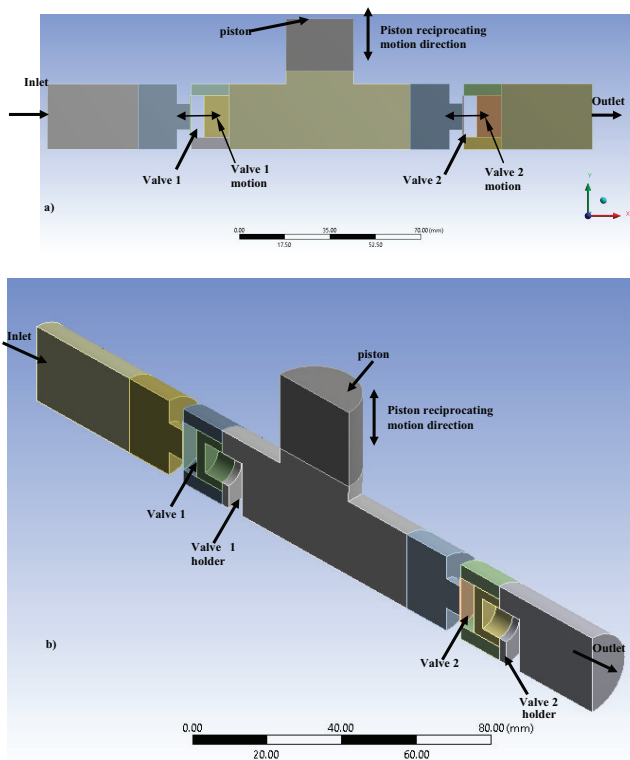


Fig. 3. Three-dimensional fluid model for reciprocating pump: (a) two-dimensional model and (b) three-dimensional model.

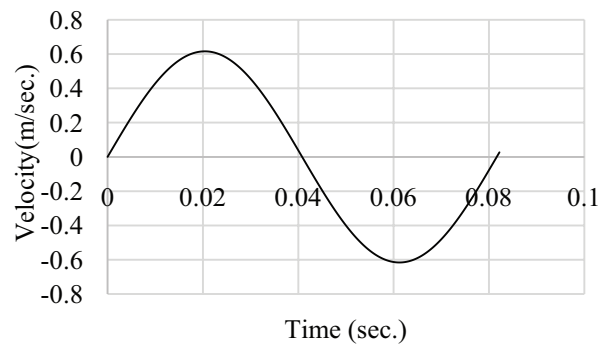


Fig. 4. Piston velocity vs. time for pump rotates at 735 rpm.

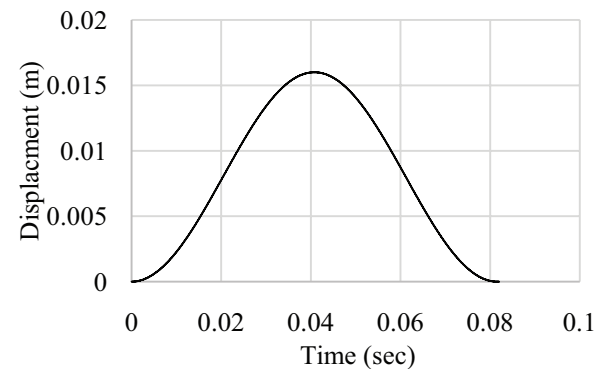


Fig. 5. Piston movement vs. time for pump rotates at 735 rpm.

of the modeling which affect the calculated parameters, and all the current results are based on the analysis of the period between 0.5 and 1.5 periodic time.

3.4. CFD results

This CFD study involves the investigation of some important operating conditions and design parameters on the volumetric efficiency of high-pressure reciprocating pump. The study includes two design parameters which are the valve spring stiffness and the valve mass. In addition, the study covers two operating condition parameters which are the piston speed and the outlet pressure. The variation of piston speed represents a simulation of the effect of using the variable frequency drive to control the pump motor speed. Furthermore, the variation of outlet pressure represents the simulation of the effect of using a throttling valve after the membrane to increase the pressure. The changing of the outlet pressure is required when the total dissolved solids (TDS) of the feed stream is increased. Before starting the CFD analysis of these parameters, the effect of mesh size on the calculated efficiency is evaluated.

3.4.1. Mesh sensitivity

The effect of mesh size on the accuracy of the calculated results is investigated for both two-dimensional and three-dimensional models. The volumetric efficiency is used as a reference to evaluate the stability of the results. The volumetric efficiency is evaluated for a selected operating point of inlet pressure 1.5 bar and outlet pressure of 60 bar and piston speed of 735 rpm at several mesh sizes. Figs. 6 and 7 show the results of the volumetric efficiency vs. the number of elements for the two-dimensional and three-dimensional model, respectively. From the results of Figs. 6 and 7, 45,000 and 200,000 elements for two-dimensional and three-dimensional model, respectively, are selected.

3.4.2. Effect of changing valve spring stiffness

The analysis results through this section involve the study of changing the valve spring stiffness on the reciprocating pump performance. Six different values of spring stiffness are used, keeping the inlet valve spring stiffness equal

to the outlet valve spring stiffness. Both two-dimensional and three-dimensional analyses are used in this study. The inlet pressure, outlet pressure, and piston speed are 1.5 bar, 60 bar, and 735 rpm, respectively. Fig. 8 shows the effect of changing the suction valve spring stiffness on the valve displacement during a complete piston stroke (periodic time = $60/735 = 0.082$ s) while Fig. 9 shows the effect of changing the exit valve spring stiffness on the valve displacement using the three-dimensional model. The results of both figures show that increasing the valve spring stiffness results in decreasing the valve displacement. The horizontal line shown in Fig. 8 at 3 mm indicates that the exit valve reaches the maximum opening stroke. The inlet and exit valve velocity profiles for selected case ($k = 1,000$ N/m) are shown in Figs. 10 and 11, respectively, for three-dimensional model. The opening of both the inlet and exit valve takes place suddenly when the hydraulic forces overcome the sum of the preload, gravity, and spring forces. This opening is characterized by fluctuations in the velocity profile. Afterwards, the velocity starts to decrease until the valve closure. The fluctuation in the valves velocity affects the flow rate profile as

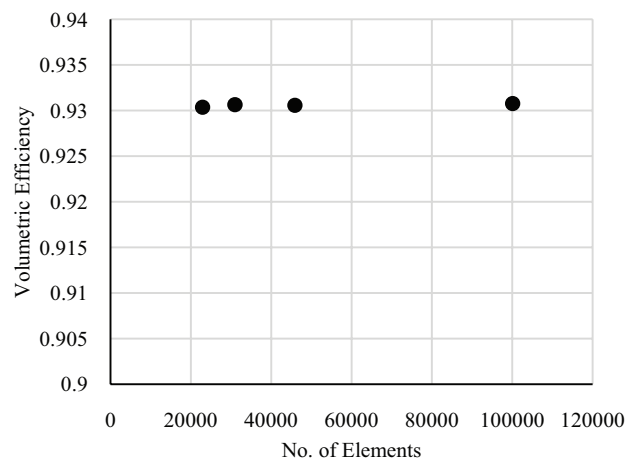


Fig. 6. Effect of mesh size on the calculated volumetric efficiency for two-dimensional model.

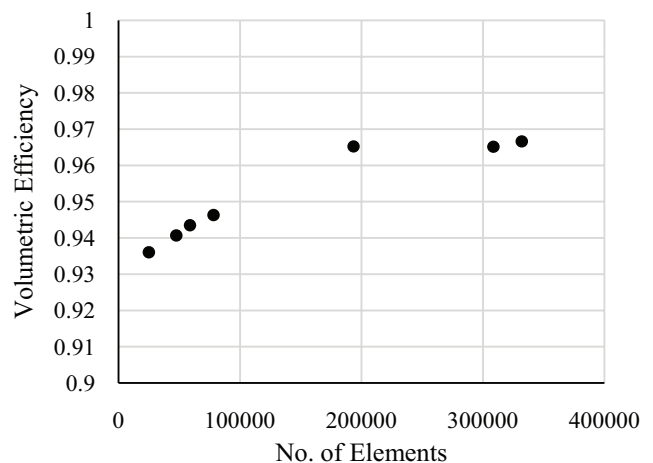


Fig. 7. Effect of mesh size on the calculated volumetric efficiency for three-dimensional model.

Table 2
Solver setup settings

Solver settings	Value
Pressure–velocity coupling	SIMPLE
Time step size	1e-5
Number of time steps	12,500
Maximum iteration	20
Convergence absolute criteria	
Continuity	0.001
x-Velocity	0.001
y-Velocity	0.001
\tilde{k}	0.001
Omega	0.001

shown in Figs. 12 and 13 in case of suction and exit valve, respectively. The negative values of flow rate shown in Fig. 12 indicate suction flow rate. The flow rate profile in both the suction and exit valve indicates that at the end of the cycle there is a reversed flow just before the valve closure.

This reversed flow is responsible for the valves volumetric efficiency. Using the CFD results, the volumetric efficiency of the pump is evaluated using Eq. (12):

$$\eta_v(\text{CFD}) = \frac{\text{Outlet volume flow rate in one cycle CFD}}{\left(\frac{\text{Piston stroke volume}}{\text{Time of one cycle}} \right)} \quad (12)$$

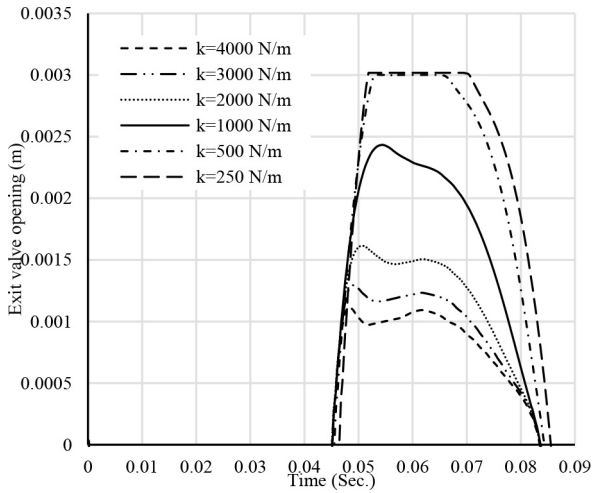


Fig. 8. Suction valve opening vs. the time in one complete cycle.

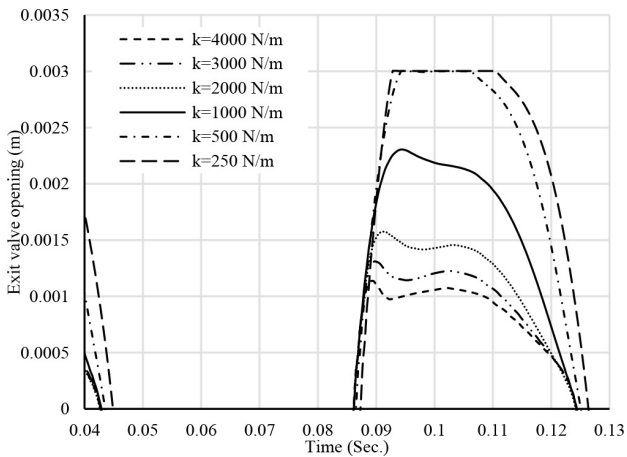


Fig. 9. Exit valve opening vs. the time in one complete cycle.

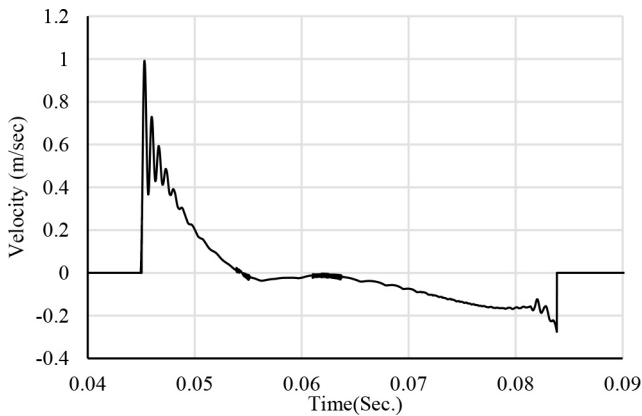


Fig. 10. Inlet valve velocity vs. the time in one complete cycle, $k = 1,000 \text{ N/m}$.

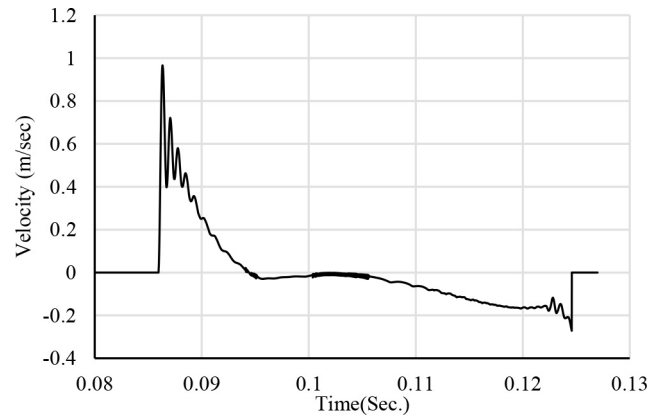


Fig. 11. Exit valve velocity vs. the time in one complete cycle, $k = 1,000 \text{ N/m}$.

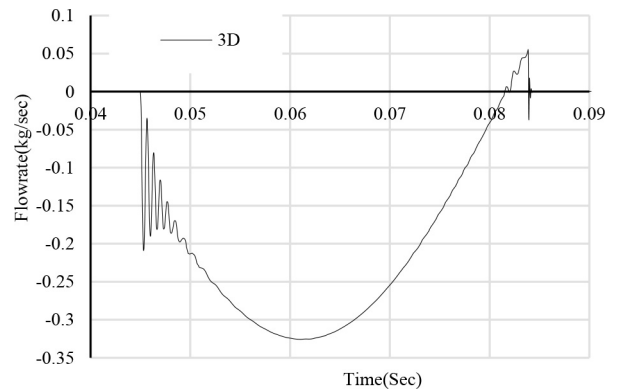


Fig. 12. Inlet flow rate vs. the time in one complete cycle, $k = 1,000 \text{ N/m}$.

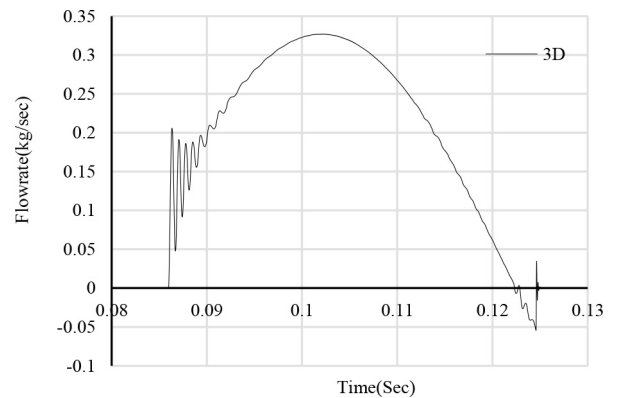


Fig. 13. Exit flow rate vs. the time in complete cycle at $k = 1,000 \text{ N/m}$.

The outlet flow rate is the sum of the positive and negative areas in Fig. 13. It is calculated per one cycle by the integration of the values of the flow rate over one cycle.

Fig. 14 shows the relation between the spring stiffness and the reciprocating pump volumetric efficiency using both two-dimensional and three-dimensional models. Both two-dimensional and three-dimensional results show that below $k = 1,000$ N/m the rate of changing the volumetric over spring stiffness increases. The rate of decreasing the volumetric efficiency with the decrease of spring stiffness below $k = 1,000$ N/m is higher in the three-dimensional model than in two-dimensional model. The difference may be referred to the different geometry between the 2D and 3D case. In the two-dimensional model, the valve model is not circular it is extruded rectangular.

3.4.3. Effect of changing valve mass

In this section, the effect of changing the valves mass on the volumetric efficiency is investigated using both two- and three-dimensional models. A range of valve masses are used from 3 to 12 g as shown in Fig. 15. These values are calculated

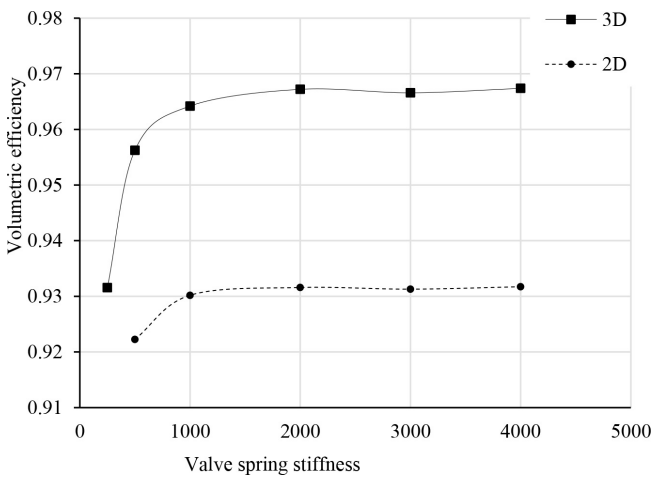


Fig. 14. Valve spring stiffness vs. valve volumetric efficiency.

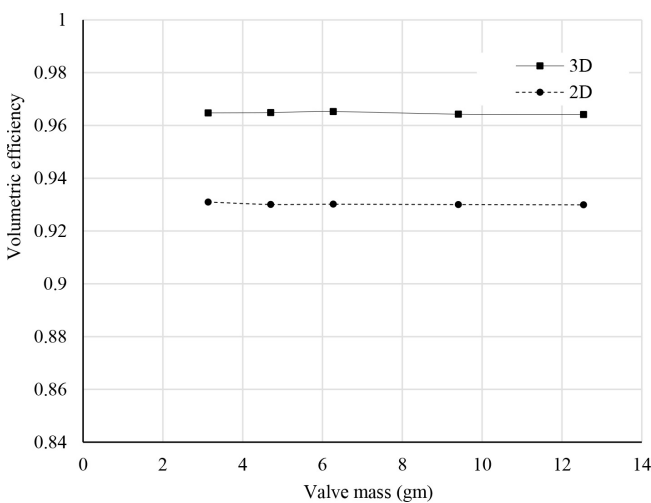


Fig. 15. Valve mass vs. the volumetric efficiency.

based on the valve dimensions with different material densities. In general, the effect of changing the valve mass on the volumetric efficiency is minor as shown in Fig. 15. Both the three-dimensional and the two-dimensional models show that increasing the valve mass approximately has no effect on the volumetric efficiency.

3.4.4. Effect of changing outlet pressure

In RO desalination plants, the outlet pressure is a function of the feedwater salinity or TDS. For this reason, the effect of changing the pump outlet pressure on the volumetric efficiency using CFD two-dimensional and three-dimensional analyses is investigated.

Fig. 16 shows the effect of changing the outlet pressure on the volumetric efficiency using both two-dimensional and three-dimensional models. The horizontal axis of Fig. 16 is present in dimensionless form as percent of full-load developed pressure. The percent of full-load developed pressure is calculated by ratio of the differential pressure to the pump frame load, see Table 1. Fig. 16 shows that for both two-dimensional and three-dimensional models, increasing the outlet pressure results in decreasing the volumetric efficiency. In addition, the results show that the effect of the outlet pressure through the full range is 2%.

3.4.5. Effect of changing the piston speed

In this section, the effect of changing the pump speed on the volumetric efficiency is investigated. Fig. 17 shows that the pump flow rate is linearly proportional to the reciprocating pump piston speed. Fig. 18 shows the relation between the pump percentage of full speed vs. the volumetric efficiency. The percentage of full speed is calculated as the ratio between the operating speed and the limit speed (see Table 1). The figure shows that increasing the pump speed results in slight reduction in the volumetric efficiency using both two- and three-dimensional models. It should be noted that the effect of piston speed in the volumetric efficiency is minor effect.

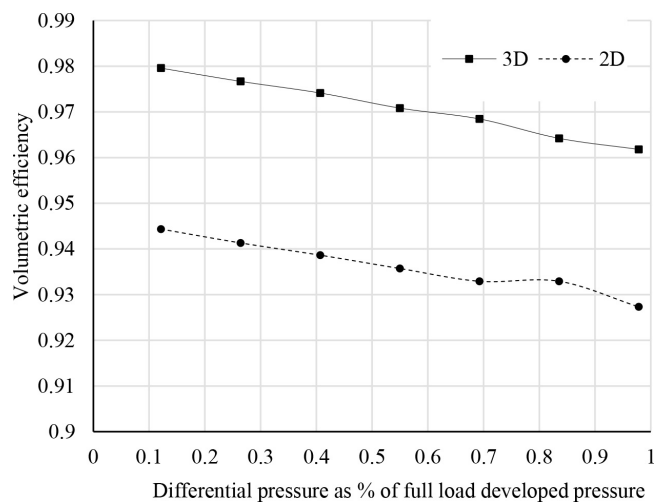


Fig. 16. Effect of changing the percentage differential pressure on the volumetric efficiency.

4. Experimental analysis and its validation

In this section, a small RO unit that utilizes a reciprocating high-pressure pump with energy recovery is considered as shown in Fig. 19. The pump is equipped with a three-phase electric motor and a timing belt to reduce the rotational

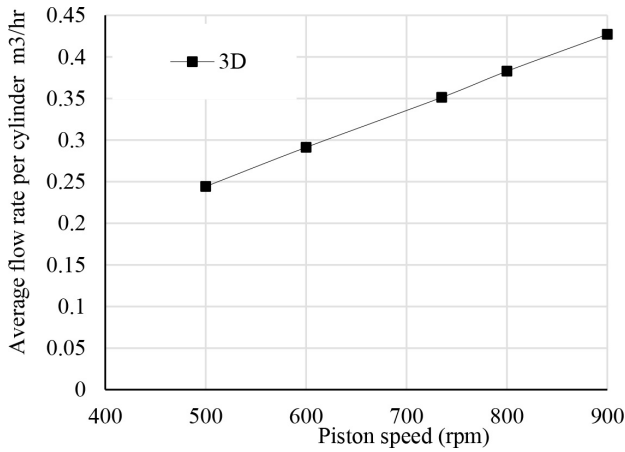


Fig. 17. Average flow rate per cylinder vs. piston speed.

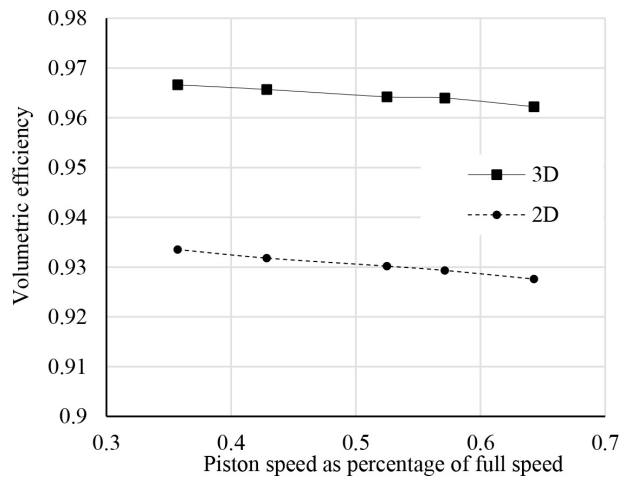


Fig. 18. Volumetric efficiency vs. the percentage of full speed.

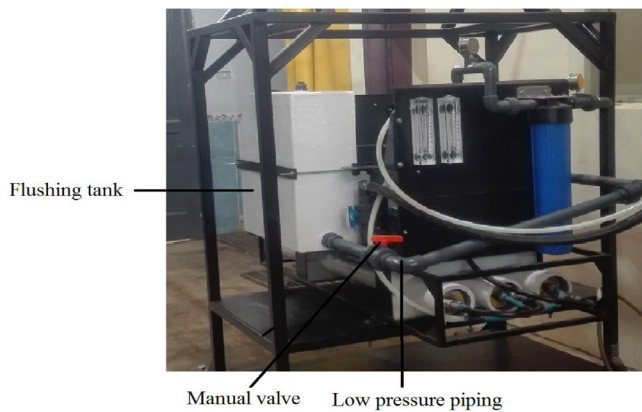


Fig. 19. The tested small RO plant.

speed from 1,725 to 735 rpm. The efficiency of the motor, η_m , at full load is 82% [3] and the efficiency of the timing belt, η_p , is 98%. The technical specifications of the plant in which this pump is equipped are listed in Table 3. Five operating conditions were conducted. These conditions were performed for different salinities of 5,000, 14,000, 18,000, 26,000, and 30,000 ppm. The feed temperature at all tests is 15°C. Feed pressure, brine pressure as well as electric power consumption in terms of current and voltage are measured. Table 4 summarizes the measurements of these tests and the associated SEC where $SEC = (\text{measured power [kW]}/\text{measured permeate flow rate [m}^3/\text{h]})$. Five parameters are measured which is the water TDS, feed pressure, brine pressure, the current at the motor supply, and the supply voltage. The electrical power in Table 4 is the product of the electrical current and the supply voltage.

Table 5 presents the elements of the reciprocating pump efficiencies at the different feed pressures. The volumetric efficiency values are based on the CFD results (see Fig. 16). The mechanical efficiency results are based on the values presented in Fig. 2. Based on the design of the reciprocating pump, 70% frame load is considered at feed pressure of 50 bar and 25% frame load is considered at feed pressure of 18 bar (see Table 1). The electrical motor efficiency is 0.82. The total pump side efficiency (η_p) is calculated according to Eq. (5).

Table 6 presented the calculated power based on the numerical model. The pump power is calculated using Eq. (3) and the data of Table 5. The recovery power is calculated using Eq. (4) and the data of Table 5. The net power is calculated according to Eq. (2). The calculated net power and the experimentally measured power are plotted vs. the feed-water TDS is in Fig. 20. The results show that the presented model is capable of accurately predicting the net power and the SEC in case of reciprocating pump with energy recovery with a maximum deviation less than 10%.

5. Conclusion

The performance of a reciprocating pump with energy recovery used in small RO plant is investigated. The investigation is based on a combination of empirical and CFD transient analysis results. The CFD analysis is performed using two- and three-dimensional reciprocating pump models. Important operating and design parameters are investigated. The operating parameters include the outlet pressure and the piston velocity. The effect of changing the outlet pressure between 10 and 70 bar (RO pressure range) on the volumetric efficiency is in the range of 2%. The piston speed is linearly proportional to the average flow rate. Increasing the piston speed from 0.35 to 0.65 of the limit speed results in reducing the volumetric efficiency by as less as 0.5%.

Table 3
Technical specifications of the RO unit

Item	Specification
Recovery ratio, %	30
Number of pressure vessels	1
Number of RO elements	3
Type of RO membrane	SW 30–4040

Table 4
Results of tests at 15°C

TDS, ppm	Feed pressure, bar	Brine pressure, bar	Current, Amp	Voltage, V	Measured power, kW	SEC, kW/m ³
5,000	18.10	17.70	3.80	228	0.8664	1.9900
14,000	30.50	29.80	4.65	226	1.0509	2.4185
18,000	35.30	34.70	5.10	228	1.1628	2.6777
26,000	45.40	44.80	5.90	228.6	1.3490	3.1113
30,000	50.10	49.80	6.25	229	1.4312	3.3033

Table 5
The values of the constituents of the pump efficiencies at different TDS

TDS, ppm	Feed pressure, bar	Volumetric efficiency, η_v	Mechanical efficiency, η_m	Electrical motor efficiency, η_e	Timing belt efficiency	Total pump side efficiency, η_p
5,000	18.1	0.977	0.7	0.82	0.98	0.563
14,000	30.5	0.974	0.78	0.82	0.98	0.626
18,000	35.3	0.972	0.83	0.82	0.98	0.666
26,000	45.4	0.970	0.85	0.82	0.98	0.683
30,000	50.1	0.968	0.86	0.82	0.98	0.691

Table 6
Calculated power efficiency based on the numerical model

TDS, ppm	Feed pressure, bar	Brine pressure, bar	Calculated pump power, kW	Calculated recovery power, kW	Net power = electrical power
5,000	18.1	17.7	1.13	0.29	0.84
14,000	30.5	29.8	1.72	0.54	1.17
18,000	35.3	34.7	1.87	0.67	1.20
26,000	45.4	44.8	2.35	0.88	1.47
30,000	50.1	49.8	2.57	0.99	1.57

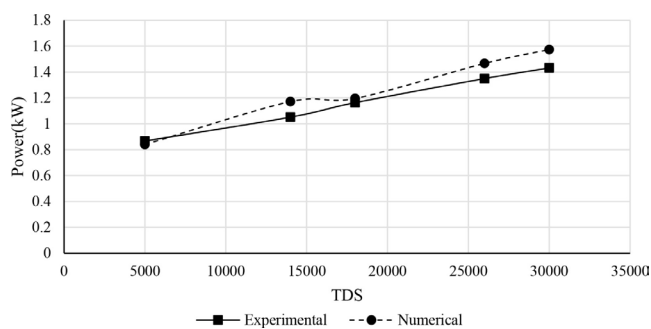


Fig. 20. Measured and calculated power vs. the feedwater TDS.

The design parameters include the valve spring stiffness and valve mass. The three-dimensional model shows that reducing the spring stiffness from 1,000 to 250 N/m results in 3% reduction in the volumetric efficiency. This indicates that poor selection of valve spring material results in a reduction in the pump performance with prolonged time. Changing the valve mass has nearly no effect on the volumetric efficiency.

The numerical simulation calculated power is compared with the experimentally measured power for the same pump. The results show that the maximum deviation is less than 10% between both results at different values of feed TDS.

Symbols

a	—	Acceleration, m/s ²
C	—	Chamber clearance volume, m ³
D	—	Displacement volume, m ³
g	—	Gravity acceleration, m/s ²
F_i	—	Preload force, N
F_g	—	Gravity force, N
F_h^g	—	Hydraulic forces, N
F_s	—	Spring force, N
H_f	—	Membrane required differential head, m
H_r	—	Brine differential head, m
H	—	Pump head, m
I	—	Electric current, Amp
k	—	Valve spring stiffness, N/m
\tilde{k}	—	Turbulence kinetic energy, η_t
m	—	Valve mass, kg
n	—	Pump rotating speed, rpm
N_s	—	Pump specific speed, $[\text{rpm}, \frac{\text{m}^3}{\text{s}}, \text{m}]$
P_{net}	—	Net power, kW
P_p	—	Pump power, kW
R_p	—	Recovery ratio, —
S	—	Check valves loss due to water slippage, —
V	—	Voltage, volts
y_v	—	Valve displacement, m

v_c	–	Water specific weight, kg/m ³
P_r	–	Energy recovery power, kW
Q_f	–	Feed flow rate, m ³ /h
Q_p	–	Permeate flow rate, m ³ /h
η_m	–	Motor efficiency, –
η_h	–	Hydraulic efficiency, –
η_p	–	Power pump overall efficiency, –
η_r	–	hydraulic efficiency of the energy recovery mechanism, –
η_t	–	transmission efficiency, –
η_v	–	pump volumetric efficiency, –
ρ_b	–	Brine density, kg/m ³
ρ_f	–	Feed density, kg/m ³
β	–	Water compressibility, Pa ⁻¹

Acknowledgment

The authors acknowledge the fund from academic of scientific research and technology (ASRT). The authors also acknowledge the Research Center and Technology Development (RCTD), Faculty of Engineering, Mataria, for enabling their computational facilities to finish this work.

References

- [1] M. Monnot, G.D.M. Carvajal, S. Laborie, C. Cabassud, R. Lebrun, Integrated approach in eco-design strategy for small RO desalination plants powered by photovoltaic energy, *Desalination*, 435 (2018) 246–258.
- [2] A.M. Bilton, R. Wiesman, A. Arif, S.M. Zubair, S. Dubowsky, On the feasibility of community-scale photovoltaic-powered reverse osmosis desalination systems for remote locations, *Renewable Energy*, 36 (2011) 3246–3256.
- [3] M. Dawoud, Economic feasibility of small scale solar powered RO desalination for brackish/saline groundwater in arid regions, *Int. J. Water Resour. Arid Environ.*, 6 (2017) 103–114.
- [4] N. Misdan, W. Lau, A. Ismail, Seawater reverse osmosis (SWRO) desalination by thin-film composite membrane—current development, challenges and future prospects, *Desalination*, 287 (2012) 228–237.
- [5] Y.C. Woo, J.J. Lee, L.D. Tijing, H.K. Shon, M. Yao, H.-S. Kim, Characteristics of membrane fouling by consecutive chemical cleaning in pressurized ultrafiltration as pre-treatment of seawater desalination, *Desalination*, 369 (2015) 51–61.
- [6] J.H. Kwon, J.H. Jung, S.R. Lee, H.W. Hur, Y. Shin, Y.H. Choi, Effects of consecutive chemical cleaning on membrane performance and surface properties of microfiltration, *Desalination*, 286 (2012) 324–331.
- [7] M. Silbernagel, T. Kuepper, E. Oklejas, Evaluation of a pressure boosting pump/turbine device for reverse osmosis energy recovery: extended testing on a seawater desalination system, *Desalination*, 88 (1992) 311–319.
- [8] F. Antunes, R. Cornman, R. Hartkopf, Centrifugal pumps for desalination, *Desalination*, 38 (1981) 109–122.
- [9] J.E. Miller, Characteristics of the Reciprocating Pump, Proceedings of the Fifth International Pump Users' Symposium, Turbomachinery Laboratory, Texas A&M Univ., College Station, TX, 1988, pp. 163–173.
- [10] A.H. Church, Centrifugal Pumps and Blowers, John Wiley & Sons, Inc., New York, 1967.
- [11] I.J. Karassik, J.P. Messina, P. Cooper, C. Heald, Pump Handbook, McGraw-Hill, New York, 1986.
- [12] P.J. Singh, N. Madavan, Complete Analysis and Simulation of Reciprocating Pumps Including System Piping, Proceedings of the fourth International Pump Symposium, 1987, pp. 53–73.
- [13] H.H. Tackett, J.A. Cripe, G. Dyson, Positive Displacement Reciprocating Pump Fundamentals – Power and Direct Acting Types, Proceedings of the 24th International Pump User Symposium, 2008, pp. 45–58.
- [14] J.J. Shu, C.R. Burrows, K.A. Edge, Pressure pulsations in reciprocating pump piping systems. Part 1: modelling, *Proc. Inst. Mech. Eng., Part I: J. Syst. Control Eng.*, 211 (1997) 229–235.
- [15] KSB, Compact High Energy System for RO Plant, *World Pumps*, 9 (2013) 27–28.
- [16] A. Bermudez-Contreras, M. Thomson, Modified operation of a small scale energy recovery device for seawater reverse osmosis, *Desal. Wat. Treat.*, 13 (2010) 195–202.
- [17] E. Hanson, M. d'Artenay, W. Childs, Energy Efficient Pumping and Energy Recovery in Desalination Sands Expo & Convention Centre, Marina Bay Sands, Water Solutions for Liveable and Sustainable Cities, GE Power & Water, 2012.
- [18] S. Arenas Urrea, F. Díaz Reyes, B. Peñate Suárez, J.A. de la Fuente Bencomo, Technical review, evaluation and efficiency of energy recovery devices installed in the Canary Islands desalination plants, *Desalination*, 450 (2019) 54–63.
- [19] S.V. Ranade, M.A. Petiwala, N. Shaikh, et al. Desalination of Brackish Water by Reverse Osmosis, 2017.
- [20] D. Song, Y. Wang, N. Lu, H. Liu, E. Xu, S. Xu, Development and stand tests of reciprocating-switcher energy recovery device for SWRO desalination system, *Desal. Wat. Treat.*, 54 (2015) 1519–1525.
- [21] J.K. Lee, J.K. Jung, J.-B. Chai, J.W. Lee, Mathematical modeling of reciprocating pump, *J. Mech. Sci. Technol.*, 29 (2015) 3141–3151.
- [22] Z. Husain, M.Z. Abdullah, Z. Alimuddin, Basic Fluid Mechanics and Hydraulic Machines, BS Publications, Hyderabad, India, 2008.
- [23] S. Wang, Improving the volumetric efficiency of the axial piston pump, *J. Mech. Design*, 134 (2012) 111001.
- [24] T.A. El-Sayed, A.A.A. Fatah, Performance of hydraulic turbocharger integrated with hydraulic energy management in SWRO desalination plants, *Desalination*, 379 (2016) 85–92.
- [25] S. Shah, S. Jain, V. Lakhera, CFD Based Flow Analysis of Centrifugal Pump, Proceedings of International Conference on Fluid Mechanics and Fluid Power, Chennai, India, paper# TM08, 2010.
- [26] A. Iannetti, M.T. Stickland, W.M. Dempster, A computational fluid dynamics model to evaluate the inlet stroke performance of a positive displacement reciprocating plunger pump, *Power Energy*, 228 (2014) 574–584.
- [27] M.J.J. Damor, D.S. Patel, K.H. Thakkar, P.K. Brahmabhatt, Experimental and CFD Analysis Of Centrifugal Pump Impeller-A Case Study, *Int. J. Eng. Res. Technol.*, 2013.
- [28] X.G. Song, L.T. Wang, Y.C. Park, W. Sun, A Fluid-structure Interaction Analysis of the Spring-loaded Pressure Safety Valve during Popping off, 14th International Conference on Pressure Vessel Technology, Shanghai, China, Procedia Engineering, 2015, pp. 87–94.
- [29] A. Budziszewski, L. Thorén, CFD Simulation of a Safety Relief Valve for Improvement of a One-Dimensional Valve Model in RELAP5, Department of Applied Physics, Chalmers University of Technology, Sweden, Gothenburg, 2012.
- [30] G. Wang, L. Zhong, X. He, Z. Lei, G. Hu, R. Li, Y. Wang, Dynamic behavior of reciprocating plunger pump discharge valve based on fluid structure interaction and experimental analysis, *PLoS One*, 10 (2015) 1–20.
- [31] M. Shojaeefard, M. Tahani, M. Ehghaghi, M. Fallahian, M. Beglari, Numerical study of the effects of some geometric characteristics of a centrifugal pump impeller that pumps a viscous fluid, *Comput. Fluids*, 60 (2012) 61–70.
- [32] J. Liu, Z. Li, L. Wang, L. Jiao, Numerical simulation of the transient flow in a radial flow pump during stopping period, *J. Fluids Eng.*, 133 (2011) 111101.
- [33] Z. Li, D. Wu, L. Wang, B. Huang, Numerical simulation of the transient flow in a centrifugal pump during starting period, *J. Fluids Eng.*, 132 (2010) 081102.